Steger, Thomas; Trimborn, Timo

Working Paper

Economic Growth and Climate Change: Many Trajectories, Many Destinations

CESifo Working Paper, No. 11053

Provided in Cooperation with:
Ifo Institute – Leibniz Institute for Economic Research at the University of Munich

Suggested Citation: Steger, Thomas; Trimborn, Timo (2024) : Economic Growth and Climate Change: Many Trajectories, Many Destinations, CESifo Working Paper, No. 11053, Center for Economic Studies and ifo Institute (CESifo), Munich

This Version is available at:
https://hdl.handle.net/10419/296142

CESifo WORKING PAPERS

11053
2024

April 2024

Economic Growth and Climate Change: Many Trajectories, Many Destinations

Thomas Steger, Timo Trimborn

CESifo

Impressum:

CESifo Working Papers
ISSN 2364-1428 (electronic version)
Publisher and distributor: Munich Society for the Promotion of Economic Research - CESifo GmbH
The international platform of Ludwigs-Maximilians University's Center for Economic Studies and the ifo Institute
Poschingerstr. 5, 81679 Munich, Germany
Telephone +49 (0)89 2180-2740, Telefax +49 (0)89 2180-17845, email office@cesifo.de
Editor: Clemens Fuest
https://www.cesifo.org/en/wp
An electronic version of the paper may be downloaded
· from the SSRN website: www.SSRN.com
· from the RePEc website: www.RePEc.org
· from the CESifo website: https://www.cesifo.org/en/wp

CESifo *Working Paper No. 11053*

Economic Growth and Climate Change: Many Trajectories, Many Destinations

Abstract

To gain insights into the mechanisms that shape the interaction between economic growth and climate change, we analyze the simplified DICE through the lens of growth theory. We analytically show that this model exhibits a continuum of saddle-point stable steady states, a property that carries over to a large set of (analytical and numerical) IAMs. This novel insight is important because it implies initial conditions of stock variables, notoriously difficult to calibrate, matter for the ultimate steady state, i.e. for the long-run economic and climate outcomes. However, we also show that a lack of information about the stock of global capital is considerably less consequential than a lack of information about GHG in the atmosphere. These properties have important implications for understanding the consequences of delayed climate policy implementation and the optimal carbon tax. We employ numerical techniques to show how a postponement of optimal climate policy implementation leads to a higher long-run temperature. We also show that the SCC-to-GDP ratio is in fact largely constant, despite transitional dynamics. However, its level depends strongly on the point in time the policy is implemented. Finally, we employ the setup to better understand the consequences of stronger TFP growth for the climate.

JEL-Codes: E100, H400, O440.

Keywords: economic growth, climate change, IAM, DICE, continuum of steady states, delayed climate policy, TFP growth, peak temperature.

Thomas Steger
Leipzig University / Germany
mtsteger@uni-leipzig.de

Timo Trimborn
Aarhus University / Denmark
tt@econ.au.dk

April 4, 2024
We thank Alkis Blanz, Simon Dietz, Reyer Gerlagh, Martin H¨ansel, Pietro Peretto, Alfred Maussner, Martin Quaas, and Sjak Smulders for valuable comments and suggestions.

1 Introduction

Integrated assessment models (IAM) enable a theory-based and quantitative analysis of economic growth and climate change. They also provide an important foundation for rational climate policy. The probably most prominent IAM is the Dynamic Integrated model of Climate and the Economy (DICE).[1] To gain insights into the mechanisms that shape the interaction between economic growth and climate change, we analyse a simplified DICE through the lens of growth theory. Viewed this way, this dynamic general equilibrium climate-economy model represents a growth model with two endogenous stock variables and two control variables, with a structure similar to many endogenous growth models (e.g., Lucas, 1988).

We analytically show that the simplified DICE exhibits a continuum of saddle-point stable steady states. We also identify exogenous technological change that drives the emission intensity asymptotically to zero as the critical assumption underlying this implication. This property carries over to a large set of (analytical and numerical) IAMs, given that many IAMs share this assumption. A continuum of steady states implies that the ultimate steady state depends on the initial stock of global capital and greenhouse gases (GHG) in the atmosphere. In general, we argue, it is important to fully understand the steady state determination as the long run has implications for the medium and short run.

The novel finding of a continuum of steady states is important for two reasons. First, calibrating IAMs requires to specify initial conditions of the stock variables. Given that the stock of global capital and the stock of GHG in the atmosphere in a given historical year are notoriously difficult to calibrate, this task is all but trivial. For instance, the IPCC (2023a) report states "Historical CO2 emissions between 1850 and 2014 have been estimated at about 2180 ± 240 GtCO2 (1-sigma range), ..." Similarly, the initial stock of global capital (K_0) is neither easily measured or calibrated. Most calibration strategies choose K_0 such that an empirically plausible capital-output ratio or real return on capital is matched. It is not surprising that the employed values vary by about 20% to 30%, as laid out below. Given the considerable uncertainty about initial stock variables, one would like to know how sensitive the final economic and climate outcome (e.g. in terms of consumption and temperature) is with respect to initial conditions. We show that a lack of information about the initial stock of capital is considerably less consequential than a lack of information about the initial stock of GHG. The reason is that the DICE inherits the neoclassical convergence mechanism from the Ramsey growth model, implying that an economy with a given initial capital stock accumulates capital faster than its hypothetical twin that has more capital to begin with. A similar mechanism does not apply to CO2. Second, and related, shocks to the stock of global capital or GHG in the atmosphere that occur along the transition to the steady state may exert a permanent impact.[2] In this sense, the global economy is stumbling into the future. We point to this implication, although we do not

[1] For the latest version of the DICE, see Barrage and Nordhaus (2023).

[2] Examples comprise volcanic eruptions, wildfires, permafrost thawing (IPCC, 2023b) or a sudden drop of emissions in a pandemic. Liu et al. (2020) report an abrupt 8.8% decrease of global CO2 emissions in the first half of 2020 compared to the same period in 2019.

model shocks explicitly.

We apply these insights to discuss three questions. 1) What are the long-term consequences of delayed climate policy implementation for economic and climate outcomes? Postponing the implementation of the (optimal) climate policy effectively means the social planner's solution starts in the future from those values of stock variables (capital and CO2) the market economy has produced so far. We numerically show that the delay of optimal climate policy implementation has comparably small economic consequences (damages, consumption). However, the long-term consequences for the climate are substantial. 2) How does a delay of climate policy implementation affect the optimal carbon tax and the SCC-to-GDP ratio? We numerically show that the point in time of optimal climate policy implementation has substantial consequences for the optimal carbon tax. The SCC-to-GDP ratio is in fact largely constant over time. However, its level increases with the delay time. 3) What is the consequence of stronger future TFP growth for the climate? We show that stronger future TFP growth shifts the entire continuum of steady states outwards. The dynamic response of GHG to an exogenous change in TFP growth is subject to opposing general equilibrium effect, implying that stronger TFP growth may in fact be a blessing for the climate.[3]

Although the finding of a continuum of steady states in prototype IAMs appears a novel insight, it is in fact not very surprising as it occurs frequently (albeit for different reasons) in growth models.[4] However, the property of a continuum of steady states is often either immaterial or not of first-order importance, as explained in section 2. In the DICE, a continuum of steady states is of first-order importance. The steady state determines final (peak) temperature and, therefore, the temperature path along the transition. The importance of the temperature level has been stressed prominently by, among others, Cai and Lontzek (2019). They investigate the consequences of climate tipping points, defined as a critical threshold at which a tiny perturbation can qualitatively alter the state or development of the climate system, for the process of economic growth and climate change.

There are two strands of related literature. First, numerical IAMs (e.g. DICE, FUND and PAGE models) are employed for policy evaluation and to provide forecasts under alternative assumptions. We contribute to this literature by clarifying how and to which extent the calibration of the initial stock of global capital and GHG in the atmosphere affect the ultimate steady state. We also show that the final steady state is more sensitive to changes of initial GHG than to changes of the initial stock of global capital. Second, analytical Integrated Assessment Models (A-IAMs) are designed to provide more transparent results than numerical IAMs. Prominent examples comprise Golosov, Hassler, Krusell, and Tsyvinski (2014), van den Bijgaart, Gerlagh, and Liski (2016), Lemoine and Rudik (2017), Gerlagh and Liski (2018), Dietz and Venmans (2019), van der Ploeg and Rezai (2019), and

[3]Forecasts on future TFP growth are extremely fragile, in contrast to population projections. Therefore, one would like to understand the implications of more or less future TFP growth.

[4]Section 4.2 elaborates on the structural sources which give rise to a continuum of steady states. It also explains why some other IAMs exhibit a unique steady state.

Traeger (2023).[5] We contribute to this literature by showing which modeling elements give rise to either a unique steady state (e.g, Dietz & Venmans, 2019; van den Bijgaart et al., 2016) or a continuum of steady states (e.g, Barrage, 2014; van der Ploeg & Rezai, 2019). This enables a better understanding of the mechanisms that shape the interaction between economic growth and climate change. Finally, Gerlagh and Keyzer (2004), employing an analytical Ramsey model augmented by a non-renewable resource with amenity value, demonstrate that delaying the implementation of an efficient resource use policy may impact the steady state resource stock, yet economic outcomes remain unaffected. Their paper comes closest to our analysis of the consequences of delayed climate policy implementation. We, in contrast, employ an explicit analytical IAM to show to which extent and how a postponement of optimal climate policy implementation further into the future affects the climate and economic outcomes.

The paper is structured as follows. Section 2 sketches the mathematical concepts which are helpful understanding the properties and implications of this class of models. Section 3 sets up the simplified DICE and provides the dynamic system that governs the evolution of the economy. Section 4 characterises analytically the continuum of steady states, identifies the critical assumption, and provides an analytical stability analysis. Section 5 employs a calibrated model, solved numerically for the big transition, to provide the foundation for the subsequent discussion. Section 6 discusses the importance of alternative initial conditions. It also investigates the consequences of delayed climate policy implementation and the consequences of stronger TFP growth for economic growth and climate change. Finally section 7 summarizes and concludes.

2 Continuum of Steady States in Growth Models

In growth theory, a continuum of steady states occurs frequently (Trimborn, 2018). However, in many cases this finding is of minor importance. To illustrate, consider the Solow growth model with exponential population growth but constant level of technology. This model exhibits a continuum of steady states for aggregate capital and GDP. The initial level of population determines to which steady state level of aggregate capital and GDP the economy converges. However, capital *per capita* and GDP *per capita* are unique in any steady state.

In contrast, a continuum of steady states may have important implications in endogenous growth models, as the steady states typically differ with respect to the level of GDP per capita (e.g., Lucas, 1988). The existence of a continuum of steady states is even more important in many climate growth models, such as the DICE, as the steady states may differ with respect to GDP per capita and temperature. We elaborate briefly, in a non-rigorous manner, on the implications of a continuum of steady states for transitional dynamics and the main economic implications.

[5] One may also count in this category the older growth models with a stock pollution and abatement as control variable (Tahvonen & Kuuluvainen, 1991; Van Der Ploeg & Withagen, 1991).

For analyzing local transitional dynamics in models exhibiting a continuum of steady states, one can apply an extension of the Hartman-Grobman theorem, namely the Center Manifold (CM) theorem (e.g., Guckenheimer & Holmes, 2002, pp. 123-128). Consider a continuum of steady states (CSS) forming a curve, labelled a (one-dimensional) manifold. We apply the CM theorem to one of these points. Consider a fixed point $\tilde{x} \in \mathbb{R}^n$ of a dynamic system $\dot{x} = f(x)$. In short, the theorem states that at a fixed point the n-dimensional space can be decomposed according to the real parts of the eigenvalues of the Jacobian matrix. According to the Hartman Grobman theorem, the eigenvectors associated with eigenvalues with negative (positive) real part span an Eigenspace tangent to a stable (unstable) manifold of that fixed point. In addition, the CM theorem states that the eigenvectors associated with an eigenvalue with zero real part span a space tangent to the center manifold.[6]

The CM theorem is usually applied to more general cases, in which the CM need not be unique and the dynamics on the CM cannot be derived from the linearized system. However, in the specific case at hand the CM is identical to the CSS. This implies the CM is unique and there is no movement along the CM.

Assume there are n_s and n_u eigenvalues with negative and positive real part, respectively, and one zero eigenvalue associated with a one-dimensional manifold of steady states, $n_s + n_u + 1 = n$. Then, we can focus on the CSS as a whole or on one point in isolation and conclude:[7]

- **Stability of the CSS**. There exist a locally unstable and stable manifold of the CSS, W^u and W^s, of dimension $n_u + 1$ and $n_s + 1$, respectively, tangent to the subspace spanned by the corresponding eigenvectors.

- **Submanifolds of the unstable and stable manifolds**. W^u and W^s are fibered by submanifolds (leaves) $W^{uu}_{\tilde{x}}$ and $W^{ss}_{\tilde{x}}$ with $\tilde{x}$ on the CSS. $W^{uu}_{\tilde{x}}$ and $W^{ss}_{\tilde{x}}$ are of dimension n_u and n_s, respectively, and tangent to the subspace spanned by the corresponding eigenvectors. All points on $W^{uu}_{\tilde{x}}$ converge to $\tilde{x}$ as $t \to -\infty$, while all points on $W^{ss}_{\tilde{x}}$ converge to $\tilde{x}$ as $t \to \infty$.

The first bullet point, a generalization of the Blanchard and Kahn (1980) conditions adapted for continuous-time systems, determines the number of initial conditions required for a unique solution. The second bullet point holds that each point ($\tilde{x}$) on the CSS is associated with a stable submanifold describing a convergence to that point ($\tilde{x}$). Taking the structure of the optimization problem into account, this implies that the (initial) state variables determine to which steady state the economy is converging.

Regarding the DICE, we show below that each steady state exhibits a different capital stock, $\tilde{K}$, and carbon stock in the atmosphere, $\tilde{S}$. This implies that the asymptotic temper-

[6]Loosely speaking, the CM is defined as the set of points $x \in \mathbb{R}^n$ such that the system stays within this set forever. The stable (unstable) manifold is the set of points $x \in \mathbb{R}^n$ such the system converges to (diverges from) the CM. See Guckenheimer and Holmes (2002) for a formal definition

[7]These conclusion can either be derived by applying the CM theorem to each point from the continuum of steady states simultaneously or by applying the Fundamental theorem of normally hyperbolic invariant manifolds (e.g., Hirsch, Pugh, & Shub, 1977; Trimborn, 2018)

ature is different for each steady state. Which steady state is ultimately realized depends on initial conditions, K_0 and S_0.

Moreover, assume an economy is converging along fibre $W^{ss}_{\tilde{x}^1}$ to the steady state $\tilde{x}^1$ on the CSS. Any shock or temporary policy which diverts the economy from $W^{ss}_{\tilde{x}^1}$ and relocates it to another fibre, say $W^{ss}_{\tilde{x}^2}$, will have a permanent impact, since the economy converges to $\tilde{x}^2$ instead of $\tilde{x}^1$. Thus, the implications for the steady state are fundamentally different to a standard neoclassical economy.

3 Model Setup

We set up a simplified DICE. The simplification concern the climate module. The modeling strategy follows the A-IAM literature (Dietz & Venmans, 2019; Golosov et al., 2014).

3.1 Social planner's problem

The social planner's problem is as follows

$$
\begin{aligned}
&\max_{[c_t,\mu_t]} \int_0^\infty \frac{c_t^{1-\varphi}-1}{1-\varphi} L_t e^{-\rho t} \mathrm{dt} \quad \text{s.t.} \\
&\quad \dot{K}_t = Q_t - \delta K_t - c_t L_t, \quad K_0: \text{ given} \\
&\quad Q_t = e^{-\frac{\gamma}{2} T_t^2} \left(1 - \theta_{1,t} \mu_t^{\theta_2}\right) Y_t \quad \text{with} \quad Y_t = A_t K_t^{\alpha} L_t^{1-\alpha} \\
&\quad T_t = \zeta S_t \\
&\quad \dot{S}_t = E_t, \quad S_0: \text{ given} \\
&\quad E_t = (1-\mu_t)\, \sigma_t Y_t,
\end{aligned}
\tag{P1}
$$

where t denotes the continuous time index, $\rho > 0$ the discount rate, $\varphi > 0$ the elasticity of marginal utility w.r.t. consumption, $\delta > 0$ the rate of capital depreciation, $\gamma \geq 0$ the damage function coefficient, $\theta_{1,t} \geq 0$ the fraction of output required to reduce emissions to zero, $\theta_2 > 1$ the abatement convexity parameter, $0 < \alpha < 1$ the capital elasticity, $\zeta \geq 0$ the temperature response coefficient, and $\sigma_t \geq 0$ the emissions intensity. The two control variables are per capita consumption (c_t) and the emission control rate (μ_t). The two state (or stock) variables are the stock of global capital (K_t) and the stock of C02 in the atmosphere (S_t). Both population and TFP follow exogenous and bounded processes, i.e. $\lim_{t\to\infty} A_t = \tilde{A}$ and $\lim_{t\to\infty} L_t = \tilde{L}$ (Barrage & Nordhaus, 2023). Moreover, the abatement cost parameter ($\theta_{1,t}$) and the emission intensity (σ_t) both converge to zero as time approaches infinity, i.e. $\lim_{t\to\infty} \theta_{1,t} = 0$ and $\lim_{t\to\infty} \sigma_t = 0$.

Two cases can be distinguished. Assuming $\theta_{1,t}$, σ_t converge exponentially to zero, the model described by (P1) is referred to as the Nordhaus case of the DICE model (Barrage & Nordhaus, 2023). Assuming $\theta_{1,t}$, σ_t are constant, the model described by (P1) is referred to as the Dietz and Venmans (2019) case.

3.2 Hamiltonian and First-order Conditions

The (current-value) Hamiltonian for (P1) and the associated first-order conditions may be expressed as follows

$$H = \frac{c_t^{1-\varphi} - 1}{1-\varphi} L_t + \lambda_t^K \left(Q_t - \delta K_t - c_t L_t\right) + \lambda_t^S (1-\mu_t)\sigma_t Y_t \tag{1}$$

$$c_t^{-\sigma} = \lambda_t^K \tag{2}$$

$$-\sigma_t \lambda_t^S = \lambda_t^K e^{-\frac{\gamma}{2}(\zeta S_t)^2} \theta_{1,t} \theta_2 \mu_t^{\theta_2 - 1} \tag{3}$$

$$\dot{\lambda}_t^K = -\lambda_t^K e^{-\frac{\gamma}{2}(\zeta S_t)^2} \left(1 - \theta_{1,t}\mu_t^{\theta_2}\right) \alpha \frac{Y_t}{K_t} + \lambda_t^K(\delta + \rho) - \lambda_t^S \left(1-\mu_t\right)\sigma_t \alpha \frac{Y_t}{K_t} \tag{4}$$

$$\dot{\lambda}_t^S = \lambda_t^K \gamma \zeta^2 S_t e^{-\frac{\gamma}{2}(\zeta S_t)^2} \left(1 - \theta_{1,t}\mu_t^{\theta_2}\right) Y_t + \lambda_t^S \rho \tag{5}$$

$$\dot{K}_t = e^{-\frac{\gamma}{2}(\zeta S_t)^2} \left(1 - \theta_{1,t}\mu_t^{\theta_2}\right) Y_t - \delta K_t - c_t L_t \tag{6}$$

$$\dot{S}_t = (1-\mu_t)\sigma_t Y_t. \tag{7}$$

Two points should be noticed. First, to simplify the analysis we do not impose the constraint $\mu_t \leq 1$.[8] We obtain very similar results if this constraint is imposed. Second, the market economy is described by ignoring the FOC for μ_t, setting $\mu_t = 0$, and setting $\lambda_t^S \left(1-\mu_t\right)\sigma_t \frac{\partial Y_t}{\partial K_t} = 0$ in (4). The transversality conditions are given as[9]

$$\lim_{t\to\infty} e^{-\rho t} \lambda_t^K K_t = 0, \quad \lim_{t\to\infty} e^{-\rho t} \lambda_t^S = 0. \tag{8}$$

The above stated system (complemented by appropriate boundary conditions) constitutes a dynamic algebraic system (DAS).[10] Its properties can be analysed by applying analytical and numerical techniques, usually applied to models of economic growth (Trimborn, 2018; Trimborn, Koch, & Steger, 2008).

4 The Long Run

Where does the economy converge to in the long run? What is the critical assumption for a possible continuum of steady states? Are these steady states saddle-point stable? This section discusses the preceding questions.

4.1 Continuum of Steady States

From the Ramsey Model we know that, given $\lim_{t\to\infty} A_t = \tilde{A}$ and $\lim_{t\to\infty} L_t = \tilde{L}$, there cannot be unbounded growth in economic variables. The stock of S_t is also bounded under the assumptions of the DICE, as explained below. However, there is not a unique steady state but rather a continuum of steady states. Given initial conditions (K_0, S_0) the economy

[8] Examples for DICE with negative emissions comprise Nordhaus (2018) and Hänsel et al. (2020).

[9] On the transversality condition on cumulative emissions see Dietz and Venmans (2019).

[10] More precisely, the underlying dynamic system represents a non-autonomous DAS due to the time-varying parameters, σ_t, A_t,L_t.

converges to a point on the following curve in (K, S) plane

$$e^{-\frac{\gamma}{2}(\zeta \tilde{S})^2} \alpha \frac{\tilde{Y}}{\tilde{K}} = \delta + \rho, \tag{CSS}$$

where $\tilde{Y} = \tilde{A}\tilde{K}^{\alpha}\tilde{L}^{1-\alpha}$. Condition (CSS) describes the continuum of steady states. This can be seen as follows. Let $g_x := \frac{\dot{x}_t}{x_t}$ denote the growth rate of any variable x_t. Then (CSS) results from $g_{\lambda^K} = 0$ together with (4), noting $\lim_{t\to\infty} \sigma_t = 0$ and $\lim_{t\to\infty} \theta_{1,t}\mu_t^{\theta_2} = 0$. This generic and well-known steady state condition states that, in the long run, the marginal product of capital (net of depreciation) must equal the time preference rate.[11]

What is the crucial assumption which gives rise to a continuum of steady states? The answer is $\lim_{t\to\infty} \sigma_t = 0$. As a result, the RHS of the $\dot{S}_t$ equation vanishes, i.e.

$$\lim_{t\to\infty} \dot{S}_t = \lim_{t\to\infty} (1 - \mu_t)\sigma_t Y_t = 0. \tag{9}$$

Notice that the RHS vanishes due to an exogenous process, σ_t. In fact, it is assumed σ_t converges sufficiently fast to zero such that S_t is bounded.[12] Hence, system (2) to (7) is under-determined. There are 6 endogenous variables $(c, \mu, \lambda^K, \lambda^S, K, S)$ and 5 equations for the determination of a steady state. What about μ_t? To see this, rewrite (3) to get

$$e^{-\frac{\gamma}{2}(\zeta S_t)^2} \frac{\theta_{1,t}\theta_2 \mu_t^{\theta_2 - 1}}{\sigma_t} = -\frac{\lambda_t^S}{\lambda_t^K}. \tag{10}$$

Given that K_t and S_t converge to constants, the RHS (the SCC in units of Q_t) must approach a constant.[13] From $\frac{\theta_{1,t}\theta_2 \mu_t^{\theta_2 - 1}}{\sigma_t}$ approaching a constant, it follows $g_{\theta_1} - g_\sigma = -(\theta_2 - 1)g_\mu$. Hence, the asymptotic constant growth rate of μ_t reads

$$\lim_{t\to\infty} g_\mu = \frac{g_{\theta_1} - g_\sigma}{1 - \theta_2}. \tag{11}$$

The long-run evolution of μ_t depends on $\frac{\theta_{1,t}}{\sigma_t}$, i.e. on the outcome of the race between the cost parameter $(\theta_{1,t})$ and the benefit parameter (σ_t) as can be seen from (3). Assume $\theta_{1,t}$ converges faster to zero than σ_t, in line with standard DICE calibrations. Plugging the numbers from Barrage and Nordhaus (2023) in, one gets $g_{\theta_1} - g_\sigma = -0.017 - (-0.015) = -0.002$. Hence, noting $1 - \theta_2 < 0$, we have $g_\mu > 0$. What about the abatement cost term $\theta_{1,t}\mu_t^{\theta_2}$ as t approaches infinity? Noting (11), the growth rate of $\theta_{1,t}\mu_t^{\theta_2}$ reads as $g_{\theta_1} + \theta_2 \frac{g_{\theta_1} - g_\sigma}{-(\theta_2 - 1)} = -0.017 - \frac{2.6}{1.6}(-0.02) < 0$. Hence, $\lim_{t\to\infty} \theta_{1,t}\mu_t^{\theta_2} = 0$. Despite the emission control rate (μ_t) increasing to infinity, the abatement cost multiplier $(1 - \theta_{1,t}\mu_t^{\theta_2})$ converges to one, i.e. abatement cost converge to zero.

[11] The economic module of the simplified DICE , given by (P1), differs only from the DICE in that it is time-continuous rather than time-discrete and in the shape of the damage function (Barrage & Nordhaus, 2023). Therefore, one can expect that a condition similar to (CSS) must hold in the DICE as well.

[12] To illustrate, integrate $\dot{S}_t = e^{g_\sigma t}(1 - e^{g_\mu t})\tilde{Y}$ with $\tilde{Y} =$ const. over t from 0 to ∞. Noting $g_\sigma < 0$, $g_\mu > 0$, and $g_\sigma + g_\mu < 0$ one sees that $\lim_{t\to\infty} S_t$ is bounded.

[13] Recall from dynamic programming that shadow prices equal derivatives of the value function w.r.t. the corresponding state variable.

4.2 Constant Emission Intensity & Full Abatement: Unique Steady State

To better understand the reason for the continuum of steady states, assume both σ and θ_1 are constant. Given that exploding S_t paths are not optimal, noting $\sigma = \text{const.}$, an optimal solution requires $\lim_{t\to\infty} \mu_t = \tilde{\mu} = 1$.[14] From (4) and (5), noting $\tilde{\mu} = 1$, one obtains the SCC in the steady state to read as

$$-\frac{\tilde{\lambda}^S}{\tilde{\lambda}^K} = \frac{\gamma\zeta^2\tilde{S}e^{-\frac{\gamma}{2}(\zeta\tilde{S})^2}(1-\theta_1)\tilde{Y}}{\rho}. \tag{12}$$

This equation specifies the carbon tax (in steady state) required to achieve full abatement in a decentralized economy. The unique steady state in terms of K_t and S_t is determined by the two following conditions

$$\underbrace{\theta_1\theta_2}_{\text{marginal cost of } \mu \text{ at } \tilde{\mu}=1} = \underbrace{\sigma\frac{\gamma\zeta^2\tilde{S}(1-\theta_1)\tilde{Y}}{\rho}}_{\text{marginal benefit of } \mu \text{ at } \tilde{\mu}=1} \tag{FA}$$

$$e^{-\frac{\gamma}{2}(\zeta\tilde{S})^2}(1-\theta_1)\alpha\frac{\tilde{Y}}{\tilde{K}} = \delta + \rho. \tag{MPK}$$

Condition (FA) results from the combination of (12) with the FOC on μ, noting $\tilde{\mu} = 1$. It describes the combinations of (K, S) such that $\tilde{\mu} = 1$ (full abatement) is indeed optimal. Condition (MPK) is basically the CSS from the simplified DICE, equation (CSS), noting that $\lim_{t\to\infty} \theta_{1,t}\mu_t^{\theta_2} = 0$ does not hold and, given $\lim_{t\to\infty} \mu_t = 1$, this term approaches θ_1. In the Nordhaus case, given $\lim_{t\to\infty} \sigma_t = 0$, $\tilde{\mu} = 1$ is not required to rule out exploding S_t paths. Therefore, condition (FA) does simply not exist.[15]

To sum up, under $\sigma = \text{const.}$ the simplified DICE exhibits a unique steady state. Optimality in this case requires that emissions endogenously land at zero asymptotically. This implies a unique long term combination of stock variables. The A-IAMs mentioned above can be categorized as follows. 1) A-IAMs with a continuum of steady states (due to exogenous and exponentially declining emission intensity): the numerically solved version of Golosov et al. (2014) model (Barrage, 2014), and the van der Ploeg and Rezai (2019) model. 2) A-IAMs with unique steady state: Dietz and Venmans (2019), van den Bijgaart et al. (2016), Li (2018).

4.3 Lessons from Eigenvalues

To analyze transitional dynamics using eigenvalue calculation, we consider the underlying dynamic system an autonomous eight-dimensional system, (4) to (7) plus dynamic equations for the time-varying variables (L_t, A_t, σ_t, $\theta_{1,t}$), with two associated algebraic

[14] Under $\sigma, \theta_1 = \text{const.}$, the simplified DICE is isomorphic to the model in Dietz and Venmans (2019), assuming no temperature delay, i.e. $T_t = \zeta S_t$. Dietz and Venmans (2019) show that exploding S_t paths violate the transversality condition on cumulative emissions. This requires, in their setup, emissions (a direct control variable) to vanish asymptotically, $\lim_{t\to\infty} E_t = 0$, which is equivalent to $\lim_{t\to\infty} \mu_t = 1$.

[15] Comparing the Nordhaus case ($\lim_{t\to\infty} \sigma_t = 0$) and the Dietz & Venmans case ($\sigma = \text{const.}$) shows there is bifurcation. The critical parameter is σ.

equations, (2) and (3). We focus on the special case $g_{\theta_1} = g_\sigma$ such that $\lim_{t\to\infty} \mu_t = \text{const.}$[16] The eigenvalues of the linearized system, evaluated at the CSS, read as (cf. appendix A.2)

$$\lambda_1 = 0, \quad \lambda_2 = \rho > 0 \tag{13}$$

$$\lambda_3 = \frac{1}{2}\left(\rho + \sqrt{\rho^2 + 4\frac{\rho + (1-\alpha)\delta}{\alpha}(\rho+\delta)(\alpha-1)(-\frac{1}{\varphi})}\right) > 0 \tag{14}$$

$$\lambda_4 = \frac{1}{2}\left(\rho - \sqrt{\rho^2 + 4\frac{\rho + (1-\alpha)\delta}{\alpha}(\rho+\delta)(\alpha-1)(-\frac{1}{\varphi})}\right) < 0 \tag{15}$$

$$\lambda_5 = g_A < 0, \quad \lambda_6 = g_L < 0, \quad \lambda_7 = g_{\theta_1} < 0, \quad \lambda_8 = g_\sigma < 0, \tag{16}$$

where g_A, g_L, g_{θ_1} and g_σ are the asymptotic rates of convergence of TFP (A_t), labor (L_t), the backstop technology ($\theta_{1,t}$), and the emission intensity (σ_t). All eigenvalues are constant along the CSS, as one would expect (Trimborn, 2018). The key takeaways can be summarized as follows:

1. **Zero eigenvalue and CSS**. The zero eigenvalue (λ_1) indicates the existence of a CSS, as explained in section 2. It results directly from $\lim_{t\to\infty} \dot{S}_t = 0$ due to $\lim_{t\to\infty} \sigma_t = 0$.

2. **Stable manifold and convergence speed**. The 5 negative eigenvalues (λ_4, λ_5, λ_6, λ_7, λ_8) indicate a (stable) manifold of dimension 6 (n_s+1 with $n_s = 5$) along which the system converges towards the CSS (cf. section 2). They also determine the speed at which the system converges, discussed numerically in section 5.3.

3. **Saddle-point stability**. There are as many jump variables (λ^K, λ^S) as unstable eigenvalues (λ_2, λ_3). Stationary equilibria on the CSS represent unique asymptotic endpoint of the transition process, conditional on K_0, S_0 and appropriate λ_0^K, λ_0^S. That is, every point on the CSS satisfies the Blanchard and Kahn (1980) conditions, implying that indeterminacy of (privately or socially) optimal solutions does not occur.

The eigenvalues are independent of the damage parameter (γ) and the temperature-carbon relation (ζ). This changes if one models a delayed temperature response by employing $\dot{T}_t = \varepsilon(\zeta S_t - T_t)$ instead of $T_t = \zeta S_t$. Dietz and Venmans (2019) assume $\varepsilon = 0.5$. In this case, there is an additional negative eigenvalue equal to (proportional to) $-\varepsilon$. Moreover, each of the stable (negative) eigenvalues can be related to a separate convergence mechanism. Specifically, eigenvalues λ_5, λ_6, λ_7, and λ_8 capture the convergence speed of TFP (g_A), labor (g_L), technological change of the backstop technology (g_{θ_1}), and emission intensity (g_σ), respectively. Eigenvalue λ_4 is the Ramsey eigenvalue describing the speed of convergence from capital accumulation.

[16] The more general case $g_\theta < g_\sigma$ such that $\lim_{t\to\infty} g_\mu = \text{const.}$ is considered in appendix A.1.

5 Transitional Dynamics

5.1 Calibration

The simplified DICE Model is calibrated at an annual frequency. The calibration of the economic module largely follows Barrage and Nordhaus (2023). The calibration of the simplified climate module follows Dietz and Venmans (2019) and Campiglio, Dietz, and Venmans (2022).

Parameter / Variable	Value	Source / Comment
ρ	0.01 per year	Barrage & Nordhaus (2023)
φ	1.35	Campiglio, Dietz & Venmans (2023, Table A1)
$\theta_{1,t}$	$0.11 \times e^{-0.017t}$	Barrage & Nordhaus (2023)
θ_2	2.6	Barrage & Nordhaus (2023)
γ	0.0077	Campiglio, Dietz & Venmans (2023, Table A1)
ζ	0.0006	Campiglio, Dietz & Venmans (2023, Table A1)
σ_t	$0.291 \times e^{-0.015t}$	Barrage & Nordhaus (2023)
α	0.3	Barrage & Nordhaus (2023)
δ	0.04	Campiglio, Dietz & Venmans (2023)
E_t^{Land}	$5.9 \times e^{-0.02t}$	Barrage & Nordhaus (2023)
S_{2020}	2000 Gt CO_2eq	Campiglio, Dietz & Venmans (2023, Table A1)
K_{2020}	300 trillion US$	matching $\frac{K}{Q} \approx 3.53$
Q_{2020}	85 trillion US$	Campiglio, Dietz & Venmans (2023, p. 18)
$L_t = L_{2020}^{(1-0.145)^t} L_\infty^{1-(1-0.145)^t}$	$L_{2020} = 7753 \times 10^6$, $L_\infty = 10825 \times 10^6$	Barrage & Nordhaus (2023)
A_{2020}	0.0279	matching $Q \approx 85 \times 10^{12}$ US$, given K, L, α, S, γ
$A_{t+1} = \frac{A_t}{1-0.0385\times\exp(-0.036\times t)}$	$\frac{A_\infty}{A_{2020}} \approx 3$	process: Barrage & Nordhaus (2023)

Table 1: Baseline calibration.

Notes: a) Barrage and Nordhaus (2023) employ $A_{t+1} = \frac{A_t}{1-0.082\times\exp(-0.0072\times 5\times t)}$ and five year time steps, implying $\frac{A_\infty}{A_{2020}} \approx 10$ and a slower rate of convergence of TFP. b) The simulation takes exogenous emissions according to E_t^{Land} into account.

5.2 Big Transition

Figure 1 displays two trajectories, projected in (K, S) plane, starting from identical initial conditions according to the baseline calibration: $K_{2020} = 300$, $S_{2020} = 2000$. The solid (dashed) curve displays the social planner solution (market economy). Both trajectories converge to different endpoints on the same CSS, displayed by the downward sloping (blue) curve on the right. The trajectories are calculated by solving the underlying dynamic system, (2) to (7) together with appropriate boundary conditions, employing the relaxation algorithm (Trimborn et al., 2008). [17]

As one would expect, the market economy (dashed) produces a higher level of cumulative CO2. This goes hand in hand with a higher global temperature, measured on the right vertical axis. Moreover, close to the CSS the market economy experiences a rising temperature and a decline of capital. It is shown below that GDP does decline as well.[18]

[17] This global solution procedure is especially suited for big transitions. Considering the first best solution, labor increases by roughly 40%, TFP by 200%, capital by 1180%, and CO2 by 110%. The relaxation algorithm is also well-suited for cases where the final steady state is not pre-determined but results as the endpoint of the transition. The algorithm is implemented in Mathematica and Matlab. The code is available at Relaxation website.

[18] The fact that the trajectory of the market economy crosses the CSS means $\lambda^K = $ const. in the respective

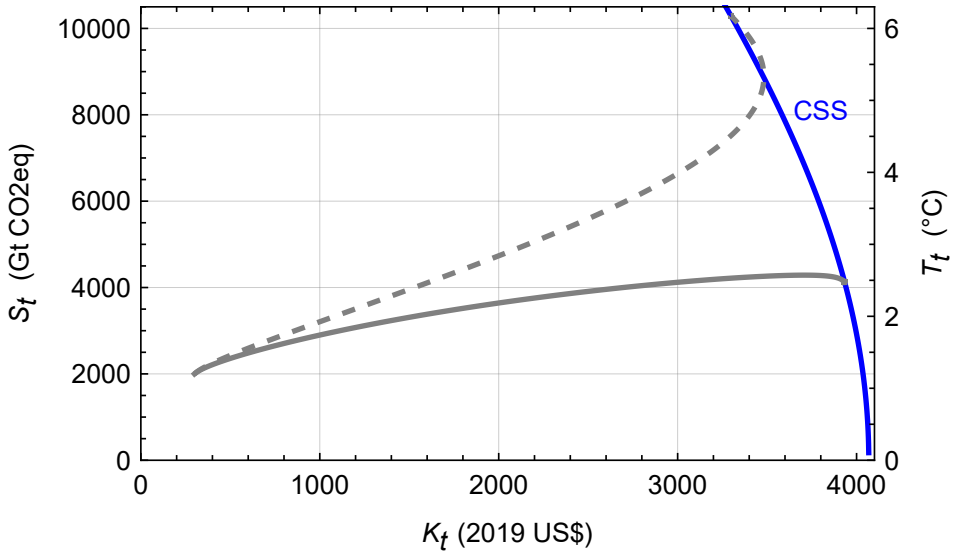

Figure 1: First-best solution & market economy.

Notes. Solid line: First-best solution. Dashed line: Market economy. Both start at $K_{2020} = 300$ trillion US$ and $S_{2020} = 2000$ Gt CO2eq according to baseline calibration. Terminal conditions employed for numerical solution are $\dot{\lambda}^K_\infty = \dot{\lambda}^S_\infty = 0$. Downward sloping (blue) curve: continuum of steady states (CSS).

5.3 Speed of Convergence

How fast does the economy converge to the steady state? Figure A.1 in appendix A.3 shows the instantaneous rates of convergence of K_t, S_t, Q_t. The initial convergence speed is about 1% (a half life of about 70 years), increases to 2.3% (half life: 23 years) and finally settles down to 1.5% (half life: 46 years). These observations are consistent with the numerical evaluations of the stable eigenvalues[19]

$$\lambda_4 \approx -0.052, \quad \lambda_5 \approx -0.036, \quad \lambda_6 \approx -0.157, \quad \lambda_7 = -0.015, \quad \lambda_8 = -0.015. \tag{17}$$

The respective eigenvalues, in general, describe movements in different directions, determined by the corresponding eigenvectors. The impact of the larger (in absolute terms) eigenvalues vanishes quickly, while the smaller (in absolute terms) eigenvalues dominate the convergence speed as time proceeds. Therefore, the smallest (in absolute terms) eigenvalue together with the associated eigenvector describe the speed at which and the direction from which the system converges asymptotically towards the CSS. The asymptotic rate of convergence, according to the calibration, is jointly determined by the speed of the backstop technology and decline rate of the emission intensity ($g_{\theta_1} = g_\sigma = -0.015$).

period. However, other variables have not reached a constant such that this point does not constitute a steady state.

[19]Notice that $\lambda_7 = \lambda_8 = -0.015$ results directly from the calibration. Moreover, λ_4 is the stable Ramsey eigenvalue. The asymptotic rates of convergence A_t and of L_t can be shown to read as $\lambda_5 = \lim_{t\to\infty} -\frac{\dot{A}_t}{A_t - A_\infty} = -0.036$ and $\lambda_6 = \lim_{t\to\infty} -\frac{\dot{L}_t}{L_t - L_\infty} = \text{Log}(1 - 0.145) \approx -0.157$.

6 Discussion

6.1 Importance of Initial Conditions

Section 2 has demonstrated that the ultimate steady state does in general depend on the initial stock of global capital and GHG in the atmosphere. We employ empirically plausible initial conditions to see the quantitative consequences of alternative initial conditions.

The initial stock of global capital (K_{2020}) as well as the initial stock of GHG in the atmosphere (S_{2020}) are notoriously difficult to quantify. For instance, the IPCC (2023a) report states "Historical CO2 emissions between 1850 and 2014 have been estimated at about 2180 ± 240 GtCO2 (1-sigma range), ..." Similarly, the stock of global capital is difficult to measure. It is therefore not surprising that global capital in a given year differs across data sources and calibrations. Barrage and Nordhaus (2023) set $K_{2020} = 302$ trillion US$ and state this value is "calibrated to give smooth interest rate path".[20] Campiglio et al. (2022, Table A1) set $K_{2020} = 348$ trillion US$, assuming the economy grows along a BGP and a capital-output ratio of 3.7. When calibrating the generalized Golosov et al. (2014) model, Barrage (2014) sets $K_0 = \alpha \frac{Y_0}{r+\delta}$ to match, given Y_0, α and δ, an annual net rate of return on capital of $r = 0.05$. As an alternative value, employed in the sensitivity analysis, she considers a K_0 that is roughly 30 % higher.

For the initial stock of GHG in the atmosphere, we consider one and two standard deviations below and above our baseline calibration, i.e. $S_{2020} \in \{1520, 1760, \underline{2000}, 2240, 2480\}$. Regarding the initial stock of global capital, we assume $\frac{K_{2020}}{Q_{2020}} \in \{2.5, 3, 3.53, 4, 4.5\}$.[21] This gives $K_{2020} \in \{212, 255, \underline{300}, 340, 383\}$.[22]

Figure 2 shows 25 trajectories starting from 25 different initial conditions (K_{2020}, S_{2020}). The pattern is remarkable. The simulation experiment traces out some stable fibres, labeled $W^{ss}_{\tilde{x}}$ in section (2), of the stable manifold, W^s. The graph illustrates that, holding S_{2020} constant, changes in K_{2020} have almost no long-run effect. In contrast, changes in S_{2020}, holding K_{2020} constant, have a strong impact, especially on $\tilde{S}$.

The economic intuition behind this pattern can be understood in two steps. First, imagine a Solovian version of the simplified DICE (constant saving rate and emission control rate). Given that the RHS of the capital accumulation equation is concave in K_t, there is the well-known neoclassical convergence mechanism. An economy with a given initial capital stock accumulates capital faster than its hypothetical twin that has more capital to begin with. Hence, there is convergence in terms of capital. In contrast, S_t does not enter the RHS of the equation of motion for CO2 such that there is no convergence in terms of S_t. This would be different if emissions were proportional to GDP net of damages. However,

[20] Source: DICE supplement, DICE2023-Excel-b-4-3-10-v18.3

[21] Feenstra, Inklaar, and Timmer (2015) report the median capital-output ratio across 142 countries (PWT 8.1) to fluctuate between 2.5 and 3.1 (1980-2011). Capital comprises structures, machinery, transport equipment, computers communication equipment, software. According to PWT 10, the capital-output ratio (rnna/rgdpna) varies between 3.3 and 4.3 (1950-2019). WID reports the global (national) wealth-to-income ratio to fluctuate between 3.7 and 6 (1995-2020); WID accessed: February 8, 2024. National wealth comprises agricultural land, housing, other domestic capital goods, net foreign assets.

[22] When changing $\frac{K_{2020}}{Q_{2020}}$, we adjust A_{2020} to keep $Q_{2020} = 85$ US$ trillion.

even if Q_t instead of Y_t were to appear on the RHS of the $\dot{S}_t$ equation, the effect would be small, given that γ is small. Moreover, additional effects kick in under endogenous controls. For instance, a higher level of S_t unfolds additional incentives to increase μ_t. This effect explains why an increase in S_0 by one unit results in a less-than-one unit permanent effect.[23]

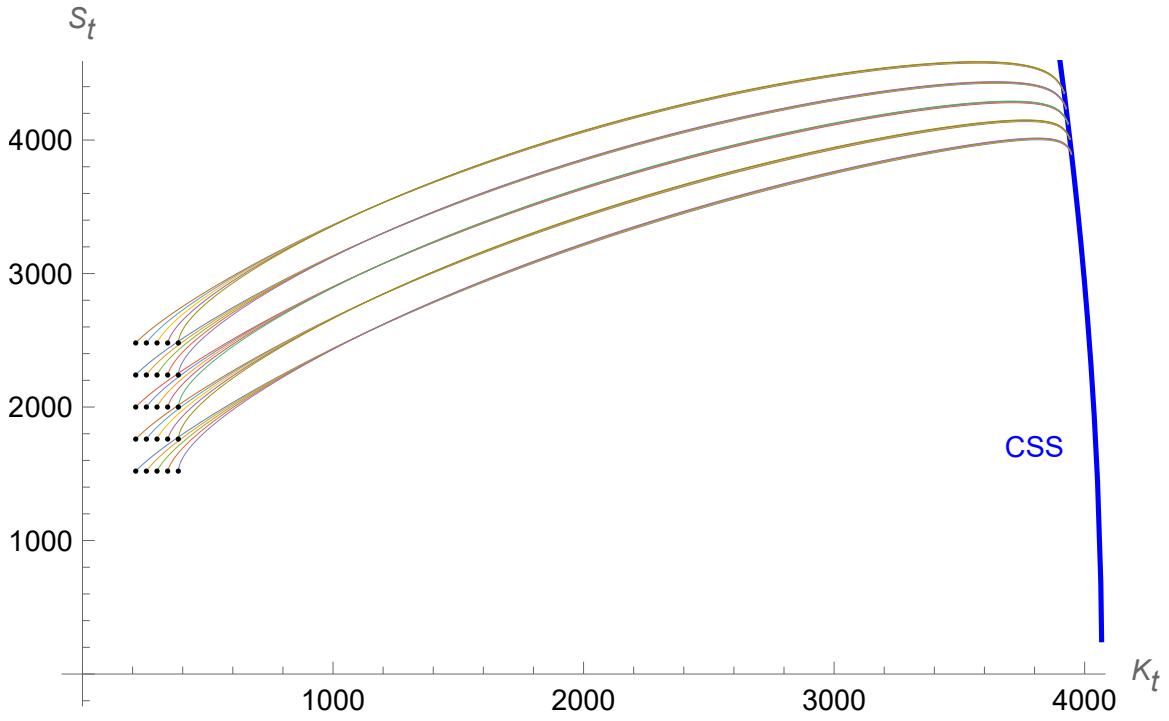

Figure 2: First-best solutions starting from grid of initial conditions.

Notes. The grid of 25 different initial conditions, i.e. values of stock variables in $t = 2020$, comprises the elements of the Cartesian product of the two sets $K_{2020} \in \{212, 255, \underline{300}, 340, 383\}$ and $S_{2020} \in \{1520, 1760, \underline{2000}, 2240, 2480\}$. Terminal conditions employed for numerical solution are $\dot{\lambda}^K_\infty = \dot{\lambda}^S_\infty = 0$. Downward sloping (blue) curve: continuum of steady states (CSS).

To sum up, changing initial K_t has a small long-run effect. The reverse holds for changes in initial S_t. This insight is important when it comes to the consequences of delayed climate policy implementation to which we turn in the next section.

6.2 Delayed Climate Policy Implementation

Postponing the implementation of the (optimal) climate policy effectively means the social planner's solution starts in the future from those values of stock variables (K, S) the market economy has produced so far. Technically speaking, the economy starts on another fibre (labeled $W^{ss}_{\tilde{x}}$ in section 2) on the stable manifold (W^s) of the social planner's solution. Hence, postponing the implementation of climate policy means the economy converges

[23]The SCC, $-\frac{\lambda^S_0}{\lambda^K_0}$, increases. This triggers an increase of μ_0, as can be seen from (3). This effect is weak, given $\gamma \approx 0.0077$ and $\theta_2 = 2.6$. A given increase in S_0 has a lower effect on $\tilde{S}$ under a higher γ (not shown).

to another steady state. This implication represents an important property of this class of IAMs. In contrast, as explained in section 4.2, a CSS does not exist in the Dietz and Venmans (2019) model, implying that postponing climate policy does not affect the ultimate steady state.

The dashed curve in Figure 3 shows the trajectory the market economy follows, starting at $K_{2020} = 300$, $S_{2020} = 2000$. The solid trajectories, starting from different positions on the market trajectory, display the social planner's solution, provided that the optimal climate policy is implemented in $t \in \{2020, 2035, 2050, ..., 2155\}$.

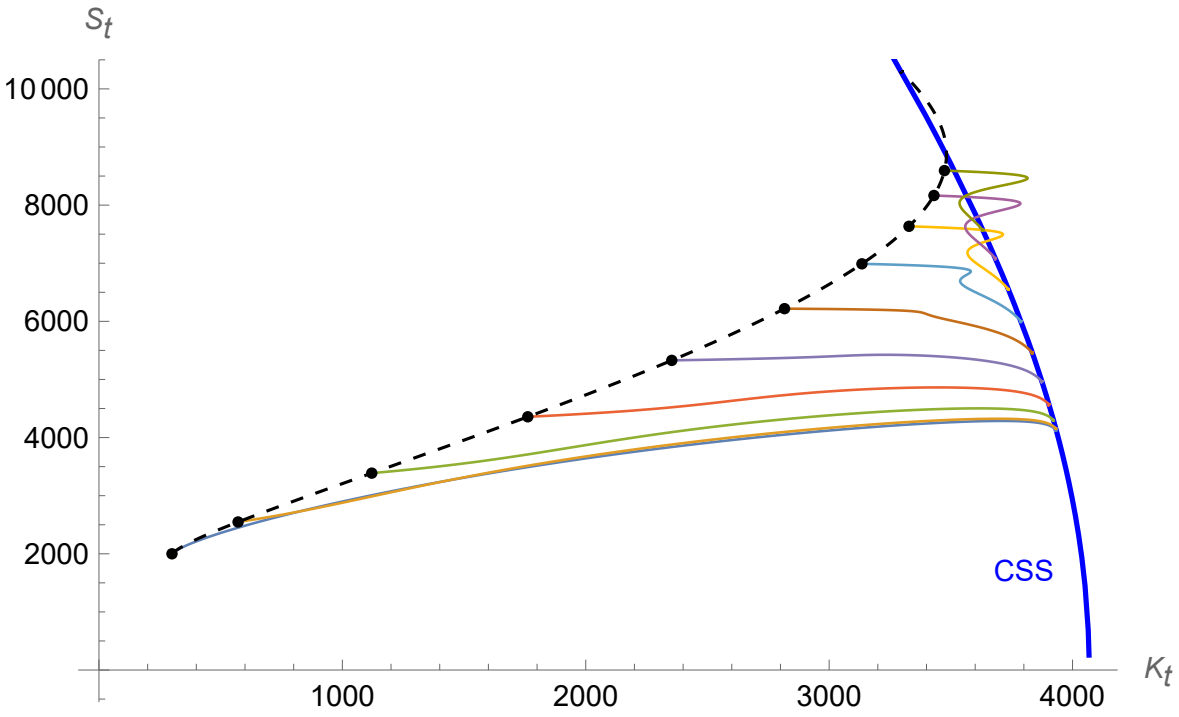

Figure 3: Delayed climate policy; trajectories in (K, S) plane.

Notes. Dashed curve: Market economy starting at $K_{2020} = 300$, $S_{2020} = 2000$ according to baseline calibration. Solid curves: First-best solutions, assuming optimal climate policy is implemented in $t \in \{2020, 2035, 2050, ..., 2155\}$. Terminal conditions employed for numerical solution are $\dot{\lambda}^K_\infty = \dot{\lambda}^S_\infty = 0$. Downward sloping (blue) curve: continuum of steady states (CSS).

Figure 4 shows the corresponding time paths for a set of endogenous variables. Again, the dashed curves depict the market economy. The solid curves show the social planner's solution, implemented in 15 year time steps. Consumption drops at the respective points in time when the (unexpected) climate policy is implemented. This is associated with a faster capital accumulation driven by a jump in λ^K_t (not shown) due to a higher than previously expected marginal product of capital. The consequences for consumption (C_t) and GDP (Q_t) are comparably small. The consequences for the temperature path (T_t) in response to delayed climate policy implementation is, however, substantial.

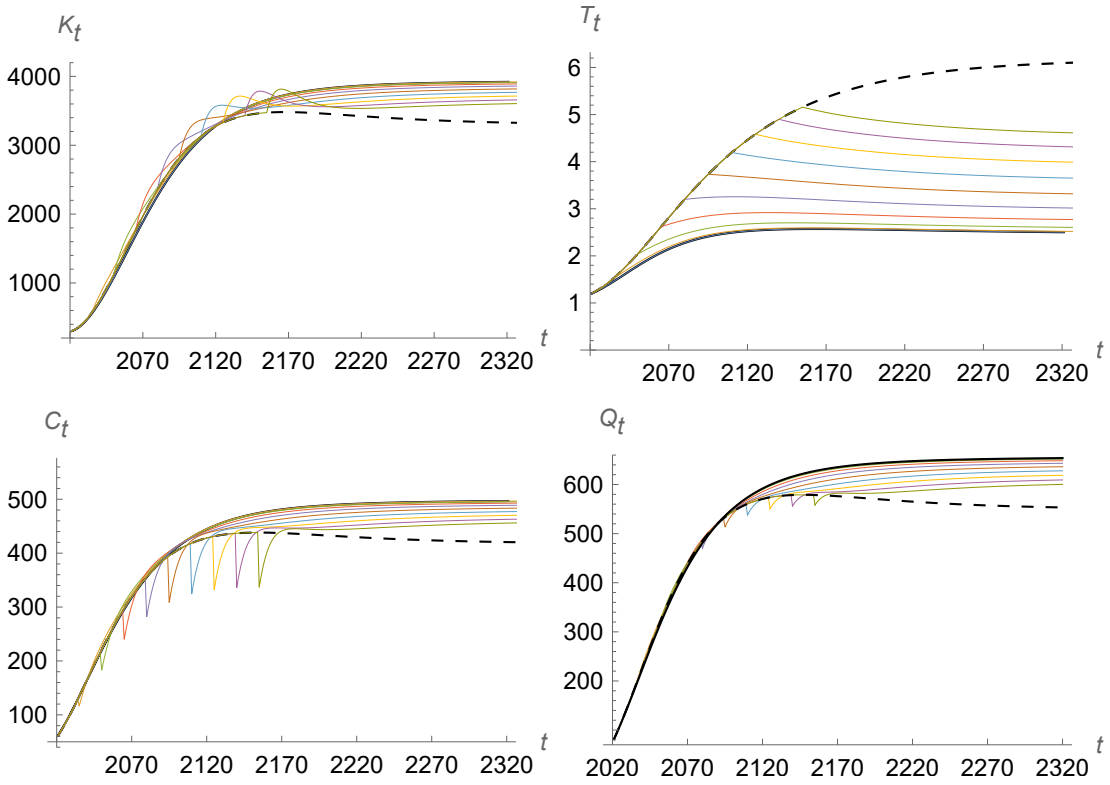

Figure 4: Delayed climate policy; time paths.

Notes. Dashed curve: Market economy starting at $K_{2020} = 300$, $S_{2020} = 2000$ according to baseline calibration. Solid curves: First-best solutions, assuming optimal climate policy is implemented in $t \in \{2020, 2035, 2050, ..., 2155\}$.

To sum up, delayed climate policy in effect means that the regulated economy starts from alternative initial conditions. If there were a unique steady state, a delay would be immaterial in the long run. However, a delay of the climate policy has long-run consequences in the simplified DICE. By backward induction, it also has consequences for the medium term. In the next section we consider the consequences of a delay for the optimal carbon tax.

6.3 Social Costs of Carbon

The social costs of carbon (SCC) provide an estimate for the optimal carbon tax. Numerical IAMs have been employed to produce numerical values for the optimal carbon tax over time (e.g., Barrage & Nordhaus, 2023). Moreover, A-IAMs have been employed to develop simple rules for the SCC.[24] A prominent example is Golosov et al. (2014) who derive a closed-form expression for a constant SCC-GDP ratio. Under a set of four assumptions, this ratio is constant despite transitional dynamics (Barrage, 2014).

[24]For an overview see Withagen (2022).

Given the existence of a CSS, one would like to know how the SCC evolve over time, assuming alternative initial conditions. We motivate the latter by considering the alternative initial conditions resulting from the experiment on delayed climate policy.

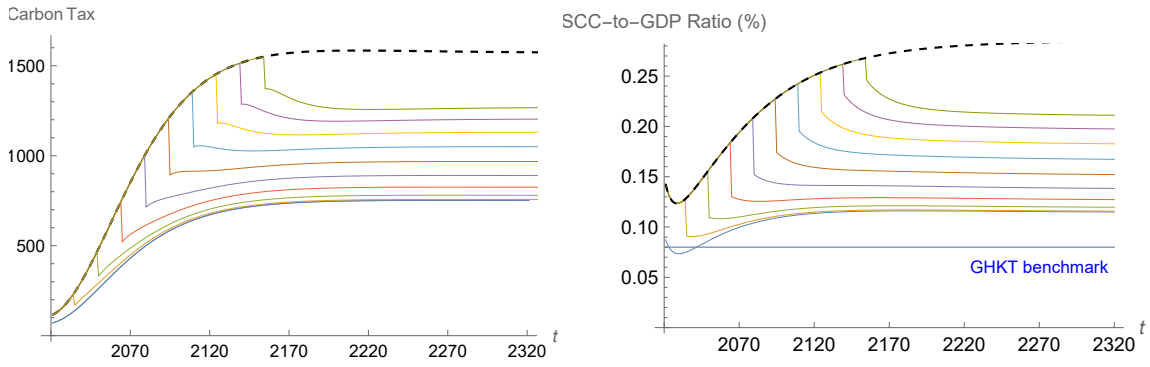

Figure 5: Optimal carbon tax (left panel) and SCC-to-GDP ratio (right panel).

Notes. a) The social costs of carbon may be defined as $\text{SCC}_t := -\frac{\lambda_t^S}{\lambda_t^K}$. Given the calibration in Table 1, it has units of measurement $\frac{10^{12}\ \text{2019 US\$}}{10^9\ \text{tCO2}}$. The left panel shows $-\frac{\lambda_t^S}{\lambda_t^K} \times 10^3$ with units $\frac{\text{2019 US\$}}{\text{tCO2}}$. b) The SCC-GDP ratio ($\frac{\text{SCC}_t}{Q_t}$) has units $\frac{1}{\text{GtCO2}}$. If, say, $\frac{\text{SCC}_t}{Q_t} = 0.0005 \frac{1}{\text{GtCO2}}$, emission of one additional GtCO2 comes with social costs of 0.05% of GDP. c) Barrage (2014) shows the benchmark in Golosov et al. (2014), abbreviated GHKT, implies a ratio of SCC to decadal gross world output equal to 8.07×10^{-5}. That is, $\frac{\text{SCC}_t}{Q_t} = 8.07 \times 10^{-4}$ for annual gross world output Q_t.

Fig. 5 (left panel) shows the time paths of the optimal carbon tax (US$ per tCO2), assuming the optimal policy is implemented in $t \in \{2020, 2035, 2050, ..., 2155\}$. The upper dashed line does not depict an optimal carbon tax, it is merely an auxiliary line showing the SCC along the market trajectory. Starting in $t = 2020$, the optimal CO2 tax starts at around 80 US$ and increases smoothly. This is somewhat higher compared to the DICE (Barrage & Nordhaus, 2023). One possible reason is that the simplified DICE assumes no delay between carbon emissions and warming.[25] Postponing the implementation of the optimal carbon tax does, however, require a substantially higher carbon tax, which may be followed by either a smooth further increase or even decrease over time, depending on the point in time of the implementation. This pattern is easily explained. The later the optimal carbon tax is implemented, the higher is S_t and K_t from which the first-best solution starts. Both variations of initial conditions imply a higher λ_t^S and a lower λ_t^K.

Fig. 5 (right panel) depicts the ratio of SCC to GDP. Golosov et al. (2014) have stressed that the SCC relative to GDP can be expressed by a simple rule and is constant over time. For comparison, the GHKT benchmark value is depicted in Fig. 5 (right panel). The paths of the SCC-to-GDP ratio illustrate that the constancy of this ratio over time appears largely consistent with the model considered here. Importantly, however, the level depends strongly on the point in time of the policy implementation, which is associated with

[25] However, Dietz and Venmans (2019) argue the slow temperature response implied by DICE is at odds with the evidence from climate science.

differing starting conditions, as explained above.

To sum up, delayed optimal climate policy implementation in effect means that the regulated economy starts from alternative initial conditions. This has important and first-order implications for the temperature path and the optimal carbon tax. In the final section we pose the opposite question. What are the consequences of a parameter change that shifts the CSS, holding initial conditions constant?

6.4 Future TFP Growth: Curse or Blessing?

What is the consequence of stronger future TFP growth for the climate? We compare our simulation results, based on the calibration in Table 1, to Barrage and Nordhaus (2023) who assume $\frac{A_\infty}{A_{2020}} \approx 10$.[26] The answer to the preceding question has two steps.

First, in the uncontrolled market economy, stronger TFP growth is a curse for the climate. This results immediately from emissions being a side product of production, as captured by $\dot{S}_t = \sigma_t Y_t$. Moreover, given that σ_t declines over time, future TFP growth is less harmful than current TFP growth.

Second, the answer is more nuanced for the optimally controlled economy for which $\dot{S}_t = (1-\mu_t)\,\sigma_t Y_t$ applies. In this case, the mechanical pollution effect described above is counteracted by more abatement of stronger future TFP growth, including possible negative emissions due to $\mu_t > 1$. That is, whether stronger TFP growth is good or bad for the climate depends on the relative importance of the mechanical pollution effect vis-a-vis the endogenous abatement effect.

Figure A.3 in appendix A.5 illustrates that stronger TFP growth may in fact be a blessing. To see why, consider the linearized FOC for μ_t[27]

$$\hat{\mu} = \left(\frac{a_{\mu\mu}}{a_\mu/\tilde{\mu}}\right)^{-1}\left(\hat{\lambda}^S + \hat{\sigma} - \hat{\lambda}^K - \frac{d_S\tilde{S}}{d}\hat{S}\right). \tag{18}$$

Future TFP growth affects μ_t via two forward-looking variables, namely λ^S and λ^K. Stronger future TFP growth increases λ^S, the NPV of marginal damages. This is the damage valuation effect. Similarly, stronger future TFP growth increases λ^K, the NPV of marginal products of capital (net of depreciation). The capital valuation effect.[28] Given that stronger TFP growth triggers additional capital accumulation, the capital valuation effect is counteracted by a decline in the marginal product of capital, which lowers the resulting rise in λ^K. This is a well-known neoclassical mechanism. The effect of a change in the SCC, $\hat{\lambda}^S - \hat{\lambda}^K$, on μ_t depends on (the inverse of) the elasticity of marginal abatement

[26] Their calibration of the process of future TFP is based on estimates from Christensen, Gillingham, and Nordhaus (2018).

[27] We focus, again, on the special case $g_\theta = g_\sigma$ such that $\lim_{t\to\infty}\mu_t = \text{const}$. A hat above a variable denotes proportional deviation from steady state. The following short-hand notation is employed $d := e^{-\frac{\gamma}{2}(\zeta S)^2}$, $a := 1-\theta_1\mu^{\theta_2}$. Moreover, $y_x := \frac{dy}{dx}$. For instance, $a_\mu = -\theta_{1,t}\theta_2\mu_t^{\theta_2-1}$.

[28] Notice that neither $\hat{\sigma}$ nor $\frac{d_S\tilde{S}}{d}\hat{S}$ are affected by stronger future TFP growth.

cost w.r.t. μ_t, given by $\left(\frac{a_{\mu\mu}}{a_\mu/\tilde{\mu}}\right)^{-1} = (\theta_2 - 1)^{-1} > 0$. For instance, $\theta_2 = 2.6$ implies a 1% increase in the SCC triggers a $1/1.6 = 0.625\%$ increase in the emission control rate.

To sum up, changes in $\tilde{A}$, $\tilde{L}$ or ρ shift the continuum of steady states, as can be seen from (CSS). The same applies to the introduction of a (distortionary) capital income tax.[29] Our analysis helps understand the response of the climate-growth model to such parameter changes.

7 Conclusions

The simplified DICE exhibits a continuum of steady states. The critical assumption underlying this implication is exogenous technological change that drives emissions to zero asymptotically, a feature shared by many IAMs. Hence, this property carries over to other (analytical and numerical) IAMs, including the numerical DICE (Barrage & Nordhaus, 2023). Experimenting with the numerical DICE, employing the provided GAMS code, supports this conclusion.

Initial conditions of stock variables, notoriously difficult to calibrate, matter for the ultimate steady state, i.e. for long-run economic and climate outcomes. However, a lack of information about the stock of global capital is considerably less consequential than a lack of information about GHG in the atmosphere. This asymmetry is rooted in the concavity of the capital accumulation equation. There is neoclassical convergence with regard to physical capital. An economy with a given amount of capital accumulates capital faster than its hypothetical twin with a larger amount of capital. A similar mechanism does not apply to the stock of CO2.

Postponing the implementation of optimal climate policy further into the future, implying the socially controlled economy starts at a later date under more capital and CO2, has comparably small economic consequences (damages, consumption). However, the long-term consequences for the climate are substantial. This would be very different in IAMs that exhibit a unique steady state. The delay of optimal climate policy implementation also has strong consequences for the optimal carbon tax. We numerically show that the SCC-to-GDP ratio is in fact largely constant over time. However, its level increases substantially with the delay time.

[29] Barrage (2019) investigates optimal carbon taxes in a dynamic general equilibrium climate-economy model with distortionary fiscal policy.

References

Barrage, L. (2014). Supplemental material, econometrica, to: Golosov et al. (2014) "optimal taxes on fossil fuel in general equilibrium". *Econometrica*, *82*(1), 41-88. Retrieved from https://onlinelibrary.wiley.com/doi/abs/10.3982/ECTA10217 doi: https://doi.org/10.3982/ECTA10217

Barrage, L. (2019, 10). Optimal Dynamic Carbon Taxes in a Climate–Economy Model with Distortionary Fiscal Policy. *The Review of Economic Studies*, *87*(1), 1-39. Retrieved from https://doi.org/10.1093/restud/rdz055 doi: 10.1093/restud/rdz055

Barrage, L., & Nordhaus, W. D. (2023, April). Policies, projections, and the social cost of carbon: Results from the dice-2023 model [Working Paper]. (31112). Retrieved from http://www.nber.org/papers/w31112 doi: 10.3386/w31112

Blanchard, O. J., & Kahn, C. M. (1980). The solution of linear difference models under rational expectations. *Econometrica*, *48*(5), 1305–1311. Retrieved 2024-02-15, from http://www.jstor.org/stable/1912186

Cai, Y., & Lontzek, T. S. (2019). The social cost of carbon with economic and climate risks. *Journal of Political Economy*, *127*(6), 2684-2734. Retrieved from https://doi.org/10.1086/701890 doi: 10.1086/701890

Campiglio, E., Dietz, S., & Venmans, F. (2022, May). Optimal climate policy as if the transition matters [Working Paper]. (10139). Retrieved from https://www.cesifo.org/en/publications/2022/working-paper/optimal-climate-policy-if-transition-matters doi: 10.3386/w31112

Christensen, P. O., Gillingham, K., & Nordhaus, W. D. (2018). Uncertainty in forecasts of long-run economic growth. *Proceedings of the National Academy of Sciences*, *115*, 5409-5414. doi: 10.1073/pnas.1713628115

Dietz, S., & Venmans, F. (2019). Cumulative carbon emissions and economic policy: In search of general principles. *Journal of Environmental Economics and Management*, *96*, 108-129. Retrieved from https://www.sciencedirect.com/science/article/pii/S0095069618302122 doi: https://doi.org/10.1016/j.jeem.2019.04.003

Feenstra, R. C., Inklaar, R., & Timmer, M. P. (2015, October). The next generation of the penn world table. *American Economic Review*, *105*(10), 3150-82. Retrieved from https://www.aeaweb.org/articles?id=10.1257/aer.20130954 doi: 10.1257/aer.20130954

Gerlagh, R., & Keyzer, M. A. (2004). Path-dependence in a ramsey model with resource amenities and limited regeneration. *Journal of Economic Dynamics and Control*, *28*(6), 1159-1184. Retrieved from https://www.sciencedirect.com/science/article/pii/S0165188903000782 doi: https://doi.org/10.1016/S0165-1889(03)00078-2

Gerlagh, R., & Liski, M. (2018). Carbon prices for the next hundred years. *The Economic Journal*, *128*(609), 728-757. Retrieved from https://onlinelibrary.wiley.com/doi/abs/10.1111/ecoj.12436 doi: https://doi.org/10.1111/

ecoj.12436

Golosov, M., Hassler, J., Krusell, P., & Tsyvinski, A. (2014). Optimal taxes on fossil fuel in general equilibrium. *Econometrica*, *82*(1), 41-88. Retrieved from https://onlinelibrary.wiley.com/doi/abs/10.3982/ECTA10217 doi: https://doi.org/10.3982/ECTA10217

Guckenheimer, J., & Holmes, P. (2002). *Nonlinear oscillations, dynamical systems, and bifurcations of vector fields* (7th ed.) (No. 42). New York: Springer.

Hirsch, M., Pugh, C., & Shub, M. (1977). *Invariant manifolds*. Springer-Verlag. Retrieved from https://books.google.de/books?id=3YGsDAEACAAJ

Hänsel, M. C., Drupp, M. A., Johansson, D. J. A., Nesje, F., Azar, C., Freeman, M. C., ... Sterner, T. (2020, 08 01). Climate economics support for the un climate targets. *Nature Climate Change*, *10*(8), 781–789. Retrieved from https://doi.org/10.1038/s41558-020-0833-x doi: 10.1038/s41558-020-0833-x

IPCC. (2023a). Climate change 2021 – the physical science basis: Working group i contribution to the sixth assessment report of the intergovernmental panel on climate change.
doi: 10.1017/9781009157896

IPCC. (2023b). Global carbon and other biogeochemical cycles and feedbacks. , 673–816.

Lemoine, D., & Rudik, I. (2017, October). Steering the climate system: Using inertia to lower the cost of policy. *American Economic Review*, *107*(10), 2947-57. Retrieved from https://www.aeaweb.org/articles?id=10.1257/aer.20150986 doi: 10.1257/aer.20150986

Li, C.-Z. (2018, February). An explicit formula for optimal carbon taxes under general economic settings [Working Paper]. (2018:1). Retrieved from https://nbn-resolving.de/urn:nbn:se:uu:diva-341099%0A

Liu, Z., Ciais, P., Deng, Z., Lei, R., Davis, S. J., Feng, S., ... others (2020). Near-real-time monitoring of global co2 emissions reveals the effects of the covid-19 pandemic. *Nature communications*, *11*(1), 5172. Retrieved from https://doi.org/10.1038/s41467-020-18922-7 doi: 10.1038/s41467-020-18922-7

Lucas, R. E. (1988). On the mechanics of economic development. *Journal of Monetary Economics*, *22*(1), 3-42. Retrieved from https://www.sciencedirect.com/science/article/pii/0304393288901687 doi: https://doi.org/10.1016/0304-3932(88)90168-7

Nordhaus, W. (2018, August). Projections and uncertainties about climate change in an era of minimal climate policies. *American Economic Journal: Economic Policy*, *10*(3), 333-60. Retrieved from https://www.aeaweb.org/articles?id=10.1257/pol.20170046 doi: 10.1257/pol.20170046

Tahvonen, O., & Kuuluvainen, J. (1991). Optimal growth with stock pollution. *Environmental Policy and the Economy*, *206*, 47–60. Retrieved 2024-01-06, from https://doi.org/10.1016/B978-0-444-88975-1.50009-8

Traeger, C. P. (2023, August). Ace—analytic climate economy. *American Economic Jour-*

nal: Economic Policy, *15*(3), 372-406. Retrieved from https://www.aeaweb.org/articles?id=10.1257/pol.20210297 doi: 10.1257/pol.20210297

Trimborn, T. (2018). On the analysis of endogenous growth models with a balanced growth path. *Journal of Mathematical Economics*, *79*, 40-50. Retrieved from https://www.sciencedirect.com/science/article/pii/S0304406818301150 doi: https://doi.org/10.1016/j.jmateco.2018.09.003

Trimborn, T., Koch, K.-J., & Steger, T. (2008). Multidimensional transitional dynamics: A simple numerical procedure. *Macroeconomic Dynamics*, *12*(3), 301–319. doi: 10.1017/S1365100507070034

van den Bijgaart, I., Gerlagh, R., & Liski, M. (2016). A simple formula for the social cost of carbon. *Journal of Environmental Economics and Management*, *77*, 75-94. Retrieved from https://www.sciencedirect.com/science/article/pii/S0095069616000061 doi: https://doi.org/10.1016/j.jeem.2016.01.005

van der Ploeg, F., & Rezai, A. (2019). Simple rules for climate policy and integrated assessment. *Environmental and Resource Economics*, *72*(1), 77–108. Retrieved from https://doi.org/10.1007/s10640-018-0280-6 doi: 10.1007/s10640-018-0280-6

Van Der Ploeg, F., & Withagen, C. (1991). Pollution control and the ramsey problem. *Environmental and Resource Economics*, *1*, 215–236. Retrieved from https://link.springer.com/article/10.1007/BF00310019#citeas doi: https://doi.org/10.1007/BF00310019

Withagen, C. (2022, Jun 01). On simple rules for the social cost of carbon. *Environmental and Resource Economics*, *82*(2), 461-481. Retrieved from https://doi.org/10.1007/s10640-022-00686-x doi: 10.1007/s10640-022-00686-x

A Appendix

A.1 Linearized system

Employing the short-hand notation $d := e^{-\frac{\gamma}{2}(\zeta S)^2}$, $a := 1 - \theta_1 \mu^{\theta_2}$, $f := AK^\alpha L^{1-\alpha}$, the Hamiltonian and first-order conditions may be expressed as

$$H = u + \lambda^K (daf - \delta K - cL) + \lambda^S (1-\mu)\sigma f \tag{19}$$

$$u_c = \lambda^K, \quad \lambda^K d a_\mu = \lambda^S \sigma \tag{20}$$

$$\dot{\lambda}^K = -\lambda^K (daf_K - \delta) - \lambda^S (1-\mu)\sigma_t f_K + \rho \lambda^K \tag{21}$$

$$\dot{\lambda}^S = -\lambda^K d_S a f + \rho \lambda^S \tag{22}$$

$$\dot{S} = (1-\mu)\sigma f \tag{23}$$

$$\dot{K} = daf - \delta K - cL, \tag{24}$$

where $f_K := \frac{\partial f}{\partial K}$ etc. Noting that A, L, σ, θ_1 are time-varying parameters, the above system constitutes a non-autonomous differential-algebraic system. When determining the eigenvalues, the processes governing these time-varying parameters must be taken explicitly into account.

Case $g_\theta = g_\sigma$: $\lim_{t\to\infty} \mu_t =$ const. Linearizing and simplifying at the steady state, the set of FOC may be expressed as

$$\begin{aligned}
\hat{c} &\cong \varphi_c \hat{\lambda}^K \\
\hat{\mu} &\cong \eta_\mu \hat{\lambda}^S + \eta_\mu \hat{\sigma} - \eta_\mu \hat{\lambda}^K - \eta_\mu \kappa_S \hat{S} \\
\dot{\hat{\lambda}}^K &\cong -\left(daf_K - \delta - \rho\right)\hat{\lambda}^K - d_S a f_K \tilde{S}\hat{S} - daf_{KK}\tilde{K}\hat{K} - daf_{KA}\tilde{A}\hat{A} - daf_{KL}\tilde{L}\hat{L} \\
\dot{\hat{\lambda}}^S &\cong -\frac{\tilde{\lambda}^K}{\tilde{\lambda}^S} d_S a f_K \hat{\lambda}^K + \rho\hat{\lambda}^S - \frac{\tilde{\lambda}^K}{\tilde{\lambda}^S} d_S a f \tilde{S}\hat{S} - \frac{\tilde{\lambda}^K}{\tilde{\lambda}^S} d_S a f_K \tilde{K}\hat{K} - \frac{\tilde{\lambda}^K}{\tilde{\lambda}^S} d_S a f_A \tilde{A}\hat{A} - \frac{\tilde{\lambda}^K}{\tilde{\lambda}^S} d_S a f_L \tilde{L}\hat{L} \\
\dot{\hat{S}} &\cong 0 \\
\dot{\hat{K}} &\cong -\frac{\tilde{c}\tilde{L}}{\tilde{K}}\varphi_c \hat{\lambda}^K + d_S a f \frac{\tilde{S}}{\tilde{K}}\hat{S} + \left(daf_K - \delta\right)\hat{K} + daf_A \frac{\tilde{A}}{\tilde{K}}\hat{A} + \left(daf_L - \tilde{c}\right)\frac{\tilde{L}}{\tilde{K}}\hat{L} \\
\dot{\hat{A}} &\cong g_A \hat{A}, \quad \dot{\hat{L}} \cong g_L \hat{L}, \quad \dot{\hat{\theta}}_1 \cong g_\theta \hat{\theta}_1, \quad \dot{\hat{\sigma}} \cong g_\sigma \hat{\sigma},
\end{aligned}$$

where $g_x = \frac{\dot{x}_t}{x_t}$, $\hat{x} := \frac{x - \tilde{x}}{x}$, $\eta_\mu := \frac{a_\mu}{a_{\mu\mu}\tilde{\mu}} > 0$, $\kappa_S := \frac{d_S \tilde{S}}{d} < 0$, $\varphi_c := \frac{u_c}{u_{cc}\tilde{c}} < 0$.

Case $g_\theta < g_\sigma$: $\lim_{t\to\infty}\mu_t = \infty$. We define $\varepsilon := (1-\mu)\sigma$ and substitute μ from the dynamic system. Linearizing and simplifying at the steady state now gives

$$\begin{aligned}
\dot{\hat{\lambda}}^K &\cong -\left(daf_K - \delta - \rho\right)\hat{\lambda}^K - d_S a f_K \tilde{S}\hat{S} - daf_{KK}\tilde{K}\hat{K} - daf_{KA}\tilde{A}\hat{A} - daf_{KL}\tilde{L}\hat{L} \\
\dot{\hat{\lambda}}^S &\cong -\frac{\tilde{\lambda}^K}{\tilde{\lambda}^S} d_S a f_K \hat{\lambda}^K + \rho\hat{\lambda}^S - \frac{\tilde{\lambda}^K}{\tilde{\lambda}^S} d_S a f \tilde{S}\hat{S} - \frac{\tilde{\lambda}^K}{\tilde{\lambda}^S} d_S a f_K \tilde{K}\hat{K} - \frac{\tilde{\lambda}^K}{\tilde{\lambda}^S} d_S a f_A \tilde{A}\hat{A} - \frac{\tilde{\lambda}^K}{\tilde{\lambda}^S} d_S a f_L \tilde{L}\hat{L} \\
\dot{\hat{S}} &\cong 0 \\
\dot{\hat{K}} &\cong -\frac{\tilde{c}\tilde{L}}{\tilde{K}}\varphi_c \hat{\lambda}^K + d_S a f \frac{\tilde{S}}{\tilde{K}}\hat{S} + \left(daf_K - \delta\right)\hat{K} + daf_A \frac{\tilde{A}}{\tilde{K}}\hat{A} + \left(daf_L - \tilde{c}\right)\frac{\tilde{L}}{\tilde{K}}\hat{L} \\
\dot{\hat{A}} &\cong g_A \hat{A}, \quad \dot{\hat{L}} \cong g_L \hat{L}, \quad \dot{\hat{\theta}}_1 \cong g_\theta \hat{\theta}_1, \quad \dot{\hat{\varepsilon}} \cong \left(\frac{\dot{\sigma}}{\sigma} + \frac{\dot{\mu}}{\mu}\right)\hat{\varepsilon} = \left(g_\sigma + \frac{g_{\theta_1} - g_\sigma}{1-\theta_2}\right)\hat{\varepsilon},
\end{aligned}$$

This system is identical to the system above except for the last equation. That is, instead of a differential equation for $\hat{\sigma}$ there is an equation for $\hat{\varepsilon}$.

A.2 Eigenvalues

Case $g_\theta = g_\sigma$: $\lim_{t\to\infty}\mu_t =$ const. The eigenvalues of the linearized system, evaluated at the CSS, read as

$$\lambda_1 = 0, \quad \lambda_2 = \rho > 0 \tag{25}$$

$$\lambda_3 = \frac{1}{2}\left(\rho + \sqrt{\rho^2 + 4\tilde{c}\tilde{L}daf_{KK}\varphi_c}\right) > 0 \tag{26}$$

$$\lambda_4 = \frac{1}{2}\left(\rho - \sqrt{\rho^2 + 4\tilde{c}\tilde{L}daf_{KK}\varphi_c}\right) < 0 \tag{27}$$

$$\lambda_5 = g_A < 0, \quad \lambda_6 = g_L < 0, \quad \lambda_7 = g_\theta < 0, \quad \lambda_8 = g_\sigma < 0 \tag{28}$$

The constancy of $\frac{\tilde{c}\tilde{L}}{\tilde{K}}$ and $adf_{KK}\tilde{K}$ results from the following observations. 1) Noting $\eta_{fK} := \frac{f_K K}{f}$, the CSS can be expressed as $da\eta_{fK}\frac{f}{K} = \rho + \delta \;\Leftrightarrow da\frac{f}{K} = \frac{\rho+\delta}{\eta_{fK}}$. From $\dot{\hat{K}} = 0$, we have $\frac{\tilde{c}\tilde{L}}{\tilde{K}} = \frac{daf}{\tilde{K}} - \delta$ and therefore $\frac{\tilde{c}\tilde{L}}{\tilde{K}} = \frac{\rho+(1-\eta_{fK})\delta}{\eta_{fK}}$. 2) Noting $\eta_{f_K K} := \frac{f_{KK}K}{f_K} < 0$ we have $f_K = \frac{f_{KK}K}{\eta_{f_K K}}$. Together with $da\frac{f}{K} = \frac{\rho+\delta}{\eta_{fK}}$, one gets $da\frac{f_{KK}K}{\eta_{f_K K}} = \rho + \delta \;\Leftrightarrow\; daf_{KK}K = (\rho+\delta)\eta_{f_K K} < 0$. 3) From $\eta_{fK} := \frac{f_K K}{f} = \alpha > 0$, $\eta_{f_K K} := \frac{f_{KK}K}{f_K} = \alpha - 1 < 0$, one obtains (14) and (15) in the main text.

Case $g_\theta < g_\sigma$: $\lim_{t\to\infty}\mu_t = \infty$. The eigenvalues are the same as before except for λ_8, which now reads as $\lambda_8 = g_\sigma + \frac{g_{\theta_1} - g_\sigma}{1-\theta_2}$.

A.3 Speed of Convergence

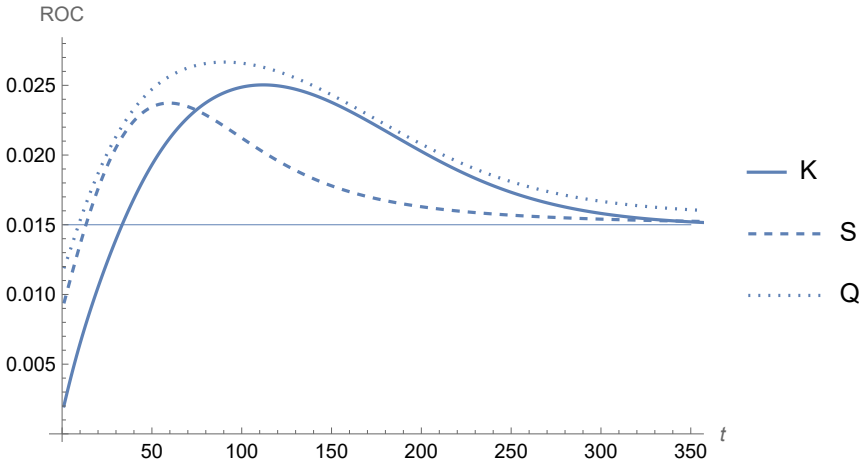

Figure A.1: Instantaneous rates convergence for K_t, S_t, Q_t.

Notes. The instantaneous rates of convergence are defined as ROC $:= -\frac{\dot{x}_t}{x_t - \bar{x}}$ for $x_t \in \{K_t, S_t, Q_t\}$. The plot is based on the numerical simulation of the dynamic system. We focus, again, on the case $g_\theta = g_\sigma = -0.015$ as the baseline calibration implies (minor) overshooting of K_t, S_t, Q_t.

A.4 Delayed Climate Policy: Emission Control Rate

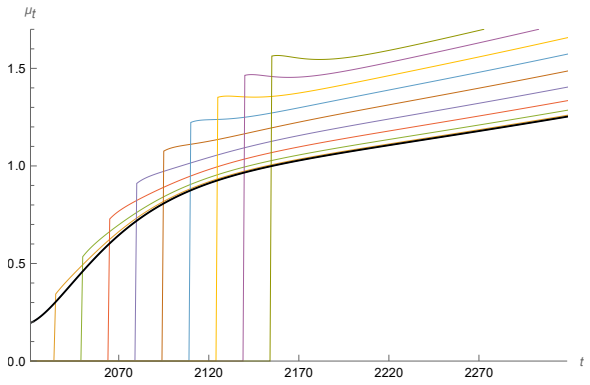

Figure A.2: Delayed climate policy: emission control rate.

Notes. The black (smooth) curve shows the emission control rate according to the social planner's solution starting right from the beginning in $t = 2020$. The remaining curves depict the emission control rates when implemented in $t \in \{2020, 2035, 2050, ..., 2155\}$.

A.5 Future TFP Growth

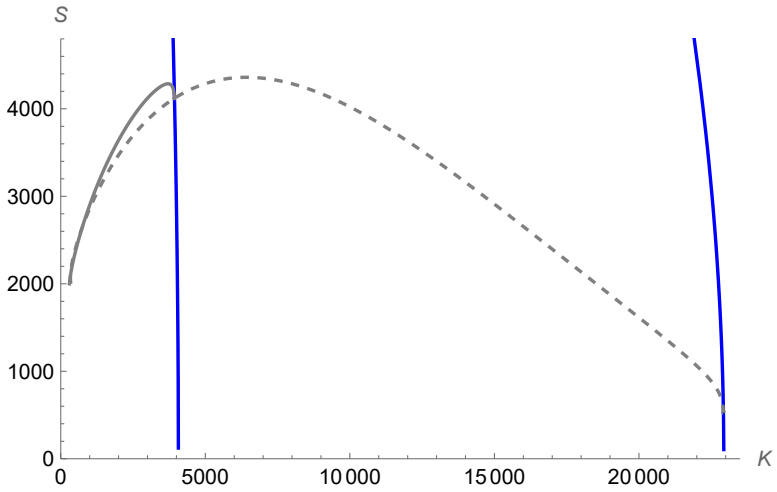

Figure A.3: Trajectories under alternative TFP growth assumptions

Notes. The solid trajectory is based on the baseline calibration, assuming $\frac{A_\infty}{A_{2020}} \approx 3$. The dashed trajectory assumes $\frac{A_\infty}{A_{2020}} \approx 10$. Barrage and Nordhaus (2023) assume TFP is governed by $A_{t+1} = \frac{A_t}{1-0.082\times\exp(-0.0072\times5\times t)}$ with $A_{2020} = 5.842$. Time step is five years. This process describes less than exponential growth, the overall increase in TFP is $\frac{A_\infty}{A_{2020}} \approx 10$. The growth rate over the first five year period is about 0.082 (an annual growth rate of about 0.082/5). It declines at a speed of 0.0072×5 (an annual speed of 0.0072) to zero.